Controlled evolution of surface patterns for ZnO coated on stretched PMMA upon thermal and solvent treatments

Yingzhi Liu[a], Haibao Lu[a,*], Ming Lei[a], Hongqiu Wei[b], Wei Min Huang[c], Jinsong Leng[b] and Yong Qing Fu[d,*]

[a] *Science and Technology on Advanced Composites in Special Environments Laboratory, Harbin Institute of Technology, Harbin 150080, People's Republic of China*

[b] *Center for Composite Materials and Structures, Harbin Institute of Technology, Harbin 150080, People's Republic of China*

[c] *School of Mechanical and Aerospace Engineering, Nanyang Technological University, 50 Nanyang Avenue, Singapore 639798*

[d] *Department of Physics and Electrical Engineering, Faculty of Engineering and Environment, University of Northumbria, Newcastle upon Tyne, NE1 8ST, UK*

[*] *Corresponding author, E-mail: luhb@hit.edu.cn and richard.fu@northumbria.ac.uk*

Abstract: Poly (methyl methacrylate) (PMMA) possesses the excellent optical properties and thermal stabilities, its shape memory effect can be triggered by heating or solvent absorption. Zinc oxide (ZnO) films, the most common semiconductor materials, were usually deposited on polymer substrates as a transparent conductive element for applications to electro-optical devices. In this paper, ZnO films with different thicknesses were deposited on PMMA substrates with different pre-strains. The

influences of the shape memory effect (SME), thermal expansion mismatch, and ethanol soaking on the evolutions of surface topographies were systematically investigated. Results revealed that the isotropic wrinkles without any preferential orientation were induced by the thermal expansion coefficient mismatch between ZnO film and PMMA substrate during annealing. The well-aligned wrinkles perpendicular to the direction of pre-strain resulted from the SME of PMMA triggered by heating. In addition, cracks appeared instead of wrinkles since the isotropic swelling of PMMA upon soaking in ethanol.

Keywords: A. Smart materials; A. Thin film; B. Surface properties; E. Heat treatment.

1. Introduction

Surface patterns induced by depositing a stiff film on the top of a compliant substrate have been extensively investigated for their potential applications in electronic devices, sensors, optical devices and actuators [1-5]. The mechanisms for producing surface patterns include wrinkling, creasing, cracking, and buckling [6-11]. Wrinkling is one of the surface buckling phenomena, which is conventionally generated in bi-layer structures consisted of a thin metallic layer and a polymer substrate. Wrinkle structures have a wide range of applications including switchable wettability, erasable systems and flexible electronics, because their significantly influences on the wettability, roughness and adhesion of the surface [3, 12-15].

Shape memory polymers (SMPs), a kind of stimulus responsive materials, have been widely studied in the past decades due to their shape memory effect (SME) [16-21]. Such smart materials are capable of fixing the pre-deformed shape under appropriate conditions, and then return from the temporary shape to the original shape under a right stimulus, such as electricity, light, heat and solvent [22-30]. Specifically, a bi-layer structure, which is composed of a mental layer and a thermally-induced, pre-stretched SMP substrate, could form complex wrinkling patterns. When it is heated and then cool down, the SME-induced compressive stress field inside the film can result in wrinkle patterns [31-33].

Compared with other kinds of SMPs, poly (methyl methacrylate) (PMMA) as a kind of physically cross-linked polymers, provide the excellent optical properties and thermal stability. Such attractive features enable its applications in solar, sensor, battery electrolytes, optical, and conductive devices [34-37]. The SME of PMMA triggered by heating or solvent absorption in small strain condition has been previously reported [38-40]. Recently, various metal and oxide films have been deposited on the PMMA substrate to achieve different functional properties (for example, optical, and electrical), and a variety of surface patterns are generated by using the SME or thermal expansion mismatch [41]. Zinc oxide (ZnO) is one of the most common semiconductor materials for applications to sensors and light emitting diodes (LEDs) [42-45]. ZnO films were usually deposited on polymer substrates as a transparent conductive element for applications such as electromagnetic shielding materials and electro-optical devices [46, 47].

ZnO film (and aluminum doped ZnO) has been frequently deposited onto PMMA to form transparent electrode. In application, electro-thermal effect would be generated on these ZnO transparent electrodes, and could trigger shape memory effect in the PMMA. Deposition of ZnO films onto PMMA could easily generate wrinkle patterns on the surface. By adjusting the film thickness or film stress appropriately, such wrinkle patterns could be significantly changed. In that case, the properties of the ZnO devices could be adjustable. In this paper, various surface wrinkling patterns were generated by coating different thicknesses of ZnO films onto pre-stretched PMMA substrates. The influences of pre-strain, post-annealing and ethanol soaking on the evolutions of surface topographies of ZnO coated on PMMA were systematically investigated.

2. Experimental procedure

PMMA sheets obtained from Ying Kwang Acrylic, Singapore, with thickness of 1 mm and glass transition temperature (T_g) of about 110°C, were used in this study. PMMA sheets were cut using a laser beam into the designed shape as shown in Fig. 1. The gauge length of the samples was set as 20 mm. The samples were uniformly pre-stretched by using the customized tensile vise into different predetermined strains (0%, 1%, 5%) at high temperature of 120°C. And then, strain was kept until it cools down to the room temperature (about 22°C), the cooling rate is 5°C/min. Subsequently, ZnO films were deposited on one side of PMMA using a magnetron sputtering equipment. Zn (99.99%) target was used during sputtering, with a DC power of 200 W and an Ar/O2 flow ratio of 50/50 SCCM (standard cubic centimeter per minute) at a gas

pressure of ~5 mTorr. In order to investigate the influence of film thicknesses on the surface morphologies, ZnO films with thicknesses varying from 5 nm to 65 nm were deposited on PMMA substrate. The thicknesses of ZnO films were tuned by changing the deposition time, and measured by a quartz crystal microbalance (QCM).

These samples of PMMA coated with ZnO film were heated to 120°C (above T_g of PMMA substrate) at a heating rate of 5°C/min and kept for 5 minutes, followed by cooling down to room temperature. Therefore, the PMMA could recovery to its original shape completely and formed surface patterns. Surface morphologies of ZnO coated on PMMA substrate were characterized using an optical microscope. The heated samples were further soaked in ethanol for different durations to study the effects of solvent-induced relaxation on the surface morphology of ZnO coated on PMMA. The pre-strains of PMMA substrates and the thicknesses of ZnO films for the samples are summarized in table 1.

3. Results and discussion

3.1. Surface morphologies

Figures 2-5 show the surface morphologies of the samples with different pre-strains (0%, 1% and 5%) and various thicknesses of ZnO film (5 nm, 15 nm, 30 nm and 45 nm), respectively. It can be found that the surface morphologies of ZnO film deposited on PMMA substrate are dependent on the thickness of ZnO film, pre-strain and heating.

Before annealing, when the film thickness is small (5 nm), no apparent wrinkles can be seen in the surface of the sample 3 (Fig. 2 (a)). Similarly, same weak surface features

could also be found on the surface of sample 1 and sample 2. The film stress in the ZnO thin layer during deposition causes the formation of these weak patterns. If the thickness of ZnO film is increased to 15 nm, sample 4 forms irregular and weak wrinkles on the surface (as shown in Fig. 3 (a)). Similarly, sample 5 and sample 6 show the same shallow wrinkles, and no significant differences appear on their surfaces, which indicate that small pre-strain has little effect on the surface topographies after film deposition at room temperature. For the samples with the film thickness of 45 nm, as illustrated in Fig. 5 (a1), it shows a large number of irregular cracks before annealing. These cracks divide the surface into several closed domains. For sample 11 (Fig. 5 (b1)), there are considerable cracks that slightly elongate along the pre-stretched direction. As shown in Fig. 5 (c1), for sample 12, there are a majority of cracks aligned along the direction of pre-strain. In these samples, pre-strain significantly influences the surface morphologies.

After annealing, many weak wrinkles perpendicular to the direction of pre-strain can be observed on the surface of sample 3 (Fig. 2 (b), thickness of ZnO film is 5 nm). For sample 1 and sample 2, the surface morphologies have very weak wrinkles after annealing. It indicated that the pre-strain has little effect on the surface pattern when the film thickness is small. From Fig. 3 (b), we can see that the disordered (isotropic) wrinkles emerge on the surface of sample 4 with the film thickness of 15 nm. The surfaces of sample 5 and sample 6 are occupied by wrinkles which are well-aligned to the perpendicular direction of the pre-strain, as shown in Fig. 3 (c) and 3 (d).

Comparing Fig. 3 (b), 3 (c) and 3 (d), it can be found that wrinkles become increasingly directional with the increase of pre-strains.

When the film thickness is increased to 30 nm, the disordered cracks emerge on the surface of sample 7 after annealing (Fig. 4 (a)), and some wrinkles scatter around the cracks. In comparison to Fig. 2 (b) and Fig. 3 (b), it can be inferred that there is a critical value (the thickness of 30 nm) at which the cracks begin to generate. For sample 8 and sample 9 after annealing (Fig. 4 (b) and 4 (c)), wrinkles are gradually disappearing, leaving only cracks along the pre-strain direction and perpendicular to the direction of the pre-strain in the surfaces.

Fig. 5 (2) represent the evolution of surface cracks as the pre-strain increased. As illustrated in Fig. 5 (a2), after annealing, sample 10 no longer shows clear wrinkles and only a large number of irregular cracks can be seen. Compared with Fig. 3 (b) and Fig. 4 (a), plenty of irregular cracks divide the surface into several closed domains when the thickness of ZnO film is beyond the critical value, 30 nm (mentioned above). With the pre-strain increased to 5%, the cracks are aligned along the direction of pre-strain increasingly. It can be concluded that initiation and evolution of the cracks depends not only on the film thickness but also on the pre-strain.

3.2. Mechanisms of the surface formation

3.2.1. Samples without pre-strain

During the deposition, plasma treatment and particle bombardment heat the surface of PMMA substrate. The difference in the thermal expansion coefficients of ZnO film and

PMMA substrate brings about a two-dimensional isotropic tensile stress in the ZnO film. This tensile stress increases as the increase of the deposition time, the thickness of ZnO film increases simultaneously. After deposition, ZnO film contracts with PMMA substrate during the samples cooling down to the room temperature, resulting in an isotropic compressive stress in the ZnO film. If the film thickness is small (5 nm and 15 nm), this tensile stress and compressive stress are too small to form visible wrinkles. Thus sample 4 forms irregular and weak wrinkles on the surface (Fig. 3 (a)). As the thickness of ZnO film increase to 45 nm, this tensile stress exceeds the fracture strength of ZnO film, and the disordered cracks emerge on the surface (as seen in Fig. 5 (a1)).

During annealing, PMMA substrate thermally expands more than ZnO film considering that PMMA substrate has a higher thermal expansion coefficient than ZnO film. Therefore, isotropic tensile stress produces in the ZnO film upon heating, and this stress evaluates with the increasing thickness of ZnO film. Therefore, ZnO film is in a two-dimensional isotropic compressive stress field when the temperature is cooled down to the room temperature. Subsequently, the resulting wrinkles are randomly distributed (as shown in Fig. 3 (b)) [11, 41, 48, 49]. The wrinkling mechanism owing to thermal expansion mismatch between ZnO film and PMMA substrate is illustrated in Fig. 6.

For the stiff film buckling on a compliant substrate under isotropic compressive stress filed, the critical wavelength of wrinkles (λ_c), the critical stress (σ_c) and the critical strain (ε_c) can be expressed as [41, 48-51]

$$\lambda_c = 2\pi t_f \left[\frac{\left(1-\upsilon_s^2\right)E_f}{3\left(1-\upsilon_f^2\right)E_s} \right]^{1/3} \approx 2\pi t_f \left(\frac{E_f}{3E_s} \right)^{1/3} \quad (1)$$

$$\sigma_c = \frac{1}{4}\left[\frac{9E_s^2 E_f}{\left(1-\upsilon_s^2\right)^2\left(1-\upsilon_f^2\right)} \right]^{1/3} \quad (2)$$

$$\varepsilon_c = \frac{1}{4}\left[\frac{3\left(1-\upsilon_f^2\right)E_s}{\left(1-\upsilon_s^2\right)E_f} \right]^{2/3} \approx \frac{1}{4}\left(\frac{3E_s}{E_f} \right)^{2/3} \quad (3)$$

Where, E_f and υ_f are Young's modulus and Poisson's ratio of ZnO film, respectively. E_s and υ_s are Young's modulus and Poisson's ratio of PMMA substrate, respectively. t_f is the thickness of ZnO film. In this work, we choose the moduli of ZnO film as E_f=104 GPa, υ_f=0.3 and PMMA substrate as E_s=4.85 MPa, υ_s=0.43 (at a full relaxation state) [41, 42, 52], respectively. The isotropic compressive stress induced by thermal expansion mismatch between the ZnO film and PMMA substrate during the annealing and cooling process result in the randomly distributed wrinkles (Fig. 3 (b)). The critical parameters of λ_c, σ_c and ε_c can be deduced by Equations 1-3. Consequently, λ_c=1.8155 μm, σ_c = 82.8652 MPa and ε_c = 0.0674%.

According to Fig. 2 (b), 3 (b) and 4 (a), there is a critical thickness of ZnO films (30 nm) to start to form cracks. The disordered cracks appear on the surface of sample 7 when the tensile stress induced by the thermal expansion mismatch between the substrate and film exceeds the fracture strength of ZnO film during annealing. This isotropic tensile stress is released by cooling after annealing, and the compression stress

forms in the ZnO film. Subsequently, wrinkles without direction scattered around the cracks. The presence of cracks alleviates this compressive stress to a certain extent and changes the stress field near the cracks. In the vicinity of the crack, the isotropic compressive stress is converted to a uniaxial compressive stress parallel to the edge of the crack [53, 54]. Consequently, some wrinkles are perpendicular to the edge of the crack near the cracks (as shown in Fig. 4(a)).

As the film thickness further increases to 45 nm, cracks spread over the entire surface and wrinkles no longer appear. During annealing, isotropic tensile stress produces in the ZnO film due to the different thermal expansion coefficients of ZnO film and PMMA substrate. The thicker the ZnO film, the greater the tensile stress. It is the reason for the increase of cracks intensity as film thickness increased. These cracks release the compressive stress in ZnO film induced by cooling, resulting in the absence of the wrinkles (similar to the wrinkles in the Fig. 4 (a)).

3.2.2. Samples with pre-strain

Since PMMA substrate is in-plain pre-stretched along one direction in this experiment, shape recovery occurs during annealing and the stored strain energy is released in the PMMA substrate. Therefore, uniaxial compressive stress along the pre-stretched direction appears in the ZnO film, resulting in the wrinkles perpendicular to the pre-stretched direction. Fig. 7 shows the mechanism of wrinkles induced by shape recovery, it illustrates that the wrinkles induced by SME perpendicular to the pre-stretched direction. In addition, the thicknesses of ZnO film and annealing have

significant effects on the surface morphologies of ZnO coated on PMMA by comparing the results of PMMA coated with 5 nm and 15 nm thickness of ZnO film. It can be summarized that small pre-strain also have an impact on wrinkles, and wrinkles become increasingly directional with the increase of pre-strain.

For the pre-stretched samples, well-aligned wrinkles (Fig. 3(c) and 3(d)) result from uniaxial compressive stress along the pre-stretched direction in the ZnO film caused by releasing the pre-strain during the shape recovery. The critical conditions in the stiff film buckling on a compliant substrate under uniaxial compressive stress filed can also be predicted by Equations 1-3. However, Equation (1) neglects the effect of Poisson's ratio, and it does not consider the influences of pre-strain. The theory considering the effect of pre-strain was established to predict the buckling of a stiff film coating on an elastic substrate at the condition of finite deformation. It was given by [12, 55]

$$\lambda = \frac{\lambda_c}{(1+\varepsilon_{pre})(1+\eta)^{1/3}} \tag{4}$$

$$\eta = \frac{5\varepsilon_{pre}(1+\varepsilon_{pre})}{32} \tag{5}$$

The average wavelength was calculated by equation (4) and experimental data, separately. The average wavelength versus the applied pre-strain is shown in Fig. 8. It indicates that the average wavelength is decreased with the pre-strain increasing.

The cracks generated in this experiment result from the thermal stress during the annealing. The pre-strain leads to cracks aligned in the direction of pre-stretching. More importantly, the larger pre-strain is, the more regular cracks are. After annealing, the number of cracks increases, and the sizes of the closed domains decreases. It can be

attributed to thermal expansion and pre-strain release of the PMMA substrate during annealing. The average length of the closed domains (L) and the average width of the closed domains (W) are shown in the Fig. 5 (a1). The aspect ratio ($R = L/W$) of closed domains on the surfaces of sample 10, sample 11 and sample 12 before annealing are measured and shown in Fig. 9. It reveals that the aspect ratio of closed domains is about linearly proportional to the pre-strain. The fitting lines are $R_{before} = 1.16 + 107.57\varepsilon$ and $R_{after} = 0.95 + 99.33\varepsilon$ for samples with 45 nm ZnO film before and after annealing, respectively. The length-width ratio of closed domains increases with the increase of pre-strain. After annealing, the slope of the fitting line decreases.

3.3. Soaking in ethanol

Fig. 10 shows the evolution of surface morphologies of sample 3, after annealing, and after soaking in ethanol for different times. The wrinkles on the surface induced by annealing (Fig. 2 (b)) become shallower after soaking for 2 hours. As the soaking time increases to 36 hours, wrinkles are less distinct and the cracks appear. It can be explained that swelling behavior caused by absorption of ethanol is isotropic, which produces tensile stress in arbitrary direction in the ZnO film. Thus, wrinkles disappear and cracks appear with the increase of soaking time.

Fig. 11 shows the evolution of surface morphologies of sample 4 and sample 6, after annealing, and after soaking in ethanol. Compare Fig. 11 (a) and Fig. 3 (b), it can be seen that the wrinkles of heated samples disappear, while a large number of disordered cracks emerge after soaking these samples in ethanol. Compare Fig. 11 (b) and Fig. 3

(d), it can be observed that many cracks perpendicular to the pre-strain instead of striped wrinkles. As the soak times increases, the width of cracks increases. It is attributed to the isotropic tensile stress produces in the ZnO film by uniform swelling of PMMA immersing in ethanol. PMMA absorbs more ethanol with the extension of soaking time. It strengthens the phenomenon of swelling and cracks become much more obvious.

Fig. 12 shows the evolution of surface morphologies of sample 10, sample 11 and sample 12, after annealing, and after soaking in ethanol. After soaking in ethanol, the difference between sample 10, sample 11 and sample 12 become obvious. The surface of sample 10 does not peel-off at all, slightly peel-off in the surface of sample 11, and seriously peel-off in the surface of sample 12. The reasons contributed to such results can be summarized two aspects. Firstly, the combined-energy-barriers between ZnO film and PMMA substrate have been significantly increased after the PMMA substrate is pre-stretched, while energy lose leads to ZnO film peel-off after soaking in ethanol. Secondly, more irregular patterns generated due to the osmotic effect, which means that for 5% pre-stretched samples, more ethanol infiltrates into the crevice between ZnO film and PMMA substrate than 0% pre-stretched samples.

4. Conclusions

In this study, we investigate the influences of the SME, thermal expansion mismatch, and ethanol soaking on the evolution of surface topographies generated by depositing the ZnO film on top of PMMA. Firstly, owing to the thermal expansion coefficients mismatch between the ZnO film and PMMA substrate, the isotropic compressive stress

generated in the ZnO film and the isotropic wrinkles formed during annealing. Furthermore, the uniaxial compressive stress produced in the ZnO film because of the SME of PMMA triggered by heating, resulting in the wrinkles perpendicular to the direction of pre-stretch. Moreover, the thicknesses of ZnO film had a significant effect on the surface morphologies, and the 30 nm was a critical thickness of ZnO film for cracking phenomenon. Finally, cracks emerged due to the isotropic tensile stress in the ZnO film induced by swelling of PMMA upon soaking in ethanol.

Acknowledgment

This work was financially supported by the National Natural Science Foundation of China (NSFC) (Grant No. 11422217, 11672642), Program for New Century Excellent Talents in University (Grant No. NCET-13-0172), Foundation for the Author of National Excellent Doctoral Dissertation of the People's Republic of China (Grant No. 201328) and National Youth Top-notch Talent Support Program.

References

[1] Stafford CM, Harrison C, Beers KL, Karim A, Amis EJ, VanLandingham MR, et al. A buckling-based metrology for measuring the elastic moduli of polymeric thin films. Nat Mater. 2004;3(8):545-50.

[2] Kim DH, Ahn JH, Choi WM, Kim HS, Kim TH, Song J, et al. Stretchable and Foldable Silicon Integrated Circuits. Science. 2008;320(25):507-11.

[3] Fu CC, Grimes A, Long M, Ferri CGL, Rich BD, Ghosh S, et al. Tunable Nanowrinkles on Shape Memory Polymer Sheets. Adv Mater. 2009;21(44):4472-6.

[4] Khang DY, Rogers JA, Lee HH. Mechanical Buckling: Mechanics, Metrology, and Stretchable Electronics. Adv Funct Mater. 2009;19(10):1526-36.

[5] Lee WK, Engel CJ, Huntington MD, Hu J, Odom TW. Controlled Three-Dimensional Hierarchical Structuring by Memory-Based, Sequential Wrinkling. Nano Lett. 2015;15(8):5624-9.

[6] Chung JY, Lee JH, Beers KL, Stafford CM. Stiffness, strength, and ductility of nanoscale thin films and membranes: a combined wrinkling-cracking methodology. Nano Lett. 2011;11(8):3361-5.
[7] Kim P, Abkarian M, StoneKim HA. Hierarchical folding of elastic membranes under biaxial compressive stress. Nat Mater. 2011;10(12):952-7.
[8] Weiss F, Cai S, Hu Y, Kang MK, Huang R, Suo Z. Creases and wrinkles on the surface of a swollen gel. J Appl Phys. 2013;114(7):073507.
[9] Cao C, Chan HF, Zang J, Leong KW, Zhao X. Harnessing localized ridges for high-aspect-ratio hierarchical patterns with dynamic tunability and multifunctionality. Adv Mater. 2014;26(11):1763-70.
[10] Chen D, Yoon J, Chandra D, Crosby AJ, Hayward RC. Stimuli-responsive buckling mechanics of polymer films. J Polym Sci, Part B: Polym Phys. 2014;52(22):1441-61.
[11] Gabardo CM, Yang J, Smith NJ, Adams-McGavin RC, Soleymani L. Programmable Wrinkling of Self-Assembled Nanoparticle Films on Shape Memory Polymers. ACS Nano. 2016;10(9):8829-36.
[12] Jiang H, Khang DY, Song J, Sun Y, Huang Y, Rogers JA. Finite deformation mechanics in buckled thin films on compliant supports. Proc Natl Acad Sci USA. 2007;104(40):15607-12.
[13] Xie T, Xiao X, Li J, Wang R. Encoding localized strain history through wrinkle based structural colors. Adv Mater. 2010;22(39):4390-4.
[14] Vajpayee S, Khare K, Yang S, Hui CY, Jagota A. Adhesion selectivity using rippled surfaces. Adv Funct Mater. 2011;21(3):547-55.
[15] Haitami AE, Bretagnol Fdr, Assuid P, Petitet G, Cantournet S, Corté L. Erasable and reversible wrinkling of halogenated rubber surfaces. Langmuir. 2013;29(50):15664-72.
[16] Lendlein A, Jiang HY, Jünger O, Langer R. Light-induced shape-memory polymers. Nature. 2005;434(7035):879-82.
[17] Behl M, Razzaq MY, Lendlein A. Multifunctional Shape‐Memory Polymers. Adv Mater. 2010;22(31):3388-10.
[18] Yao Y, Wei H, Wang J, Lu H, Leng J, Hui D. Fabrication of hybrid membrane of electrospun polycaprolactone and polyethylene oxide with shape memory property. Compos Part B: Eng. 2015;83:264-9.
[19] Zhao Q, Qi HJ, Xie T. Recent progress in shape memory polymer: New behavior, enabling materials, and mechanistic understanding. Prog Polym Sci. 2015;49:79-120.
[20] Lu H, Lei M, Zhao C, Yao Y, Gou J, Hui D, et al. Controlling Au electrode patterns for simultaneously monitoring electrical actuation and shape recovery in shape memory polymer. Compos Part B: Eng. 2015;80:37-42.
[21] Hager MD, Bode S, Weber C, Schubert US. Shape memory polymers: Past, present and future developments. Prog Polym Sci. 2015;49:3-33.
[22] Liu Y, Boyles JK, Genzer J, Dickey MD. Self-folding of polymer sheets using local light absorption. Soft matter. 2012;8(6):1764-69.
[23] Lu H, Yao Y, Huang WM, Leng J, Hui D. Significantly improving infrared

light-induced shape recovery behavior of shape memory polymeric nanocomposite via a synergistic effect of carbon nanotube and boron nitride. Compos Part B: Eng. 2014;62:256-61.
[24] Lu H, Yao Y, Huang WM, Hui D. Noncovalently functionalized carbon fiber by grafted self-assembled graphene oxide and the synergistic effect on polymeric shape memory nanocomposites. Compos Part B: Eng. 2014;67:290-5.
[25] Lu H, Liang F, Yao Y, Gou J, Hui D. Self-assembled multi-layered carbon nanofiber nanopaper for significantly improving electrical actuation of shape memory polymer nanocomposite. Compos Part B: Eng. 2014;59:191-5.
[26] Xiao R, Guo J, Safranski DL, Nguyen TD. Solvent-driven temperature memory and multiple shape memory effects. Soft matter. 2015;11(20):3977-85.
[27] Lu H, Wang X, Yao Y, Gou J, Hui D, Xu B, et al. Synergistic effect of siloxane modified aluminum nanopowders and carbon fiber on electrothermal efficiency of polymeric shape memory nanocomposite. Compos Part B: Eng. 2015;80:1-6.
[28] Lu H, Lu C, Huang WM, Leng J. Quantitative separation of the influence of copper (II) chloride mass migration on the chemo-responsive shape memory effect in polyurethane shape memory polymer. Smart Mater Struct. 2016;25(10):105003.
[29] Lu H, Yu K, Huang WM, Leng J. On the Takayanagi principle for the shape memory effect and thermomechanical behaviors in polymers with multi-phases. Smart Mater Struct. 2016;25(12):125001.
[30] Lu H, Yin J, Xu B, Gou J, Hui D, Fu Y. Synergistic effects of carboxylic acid-functionalized carbon nanotube and nafion/silica nanofiber on electrical actuation efficiency of shape memory polymer nanocomposite. Compos Part B: Eng. 2016;100:146-51.
[31] Chen Z, Young Kim Y, Krishnaswamy S. Anisotropic wrinkle formation on shape memory polymer substrates. J Appl Phys. 2012;112(12):124319.
[32] Li JJ, An YH, Huang R, Jiang HQ, Xie T. Unique aspects of a shape memory polymer as the substrate for surface wrinkling. ACS Applied Materials Interfaces. 2012;4(2):598-03.
[33] Lu H, Liu Y, Xu BB, Hui D, Fu YQ. Spontaneous biaxial pattern generation and autonomous wetting switching on the surface of gold/shape memory polystyrene bilayer. Compos Part B: Eng. 2017;122:9-15.
[34] Adhikari B, Majumdar S. Polymers in sensor applications. Prog Polym Sci. 2004;29(7):699-766.
[35] Zhao Y, Wang CC, Huang WM, Purnawali H, An L. Formation of micro protrusive lens arrays atop poly(methyl methacrylate). Opt Express. 2011;19(27):26000-05.
[36] Zhao Y, Wang CC, Huang WM, Purnawali H. Ethanol Induced Shape Recovery and Swelling in Poly(methyl methacrylate) and Applications in Fabrication of Microlens Array. Adv Sci Technol. 2012;77:354-8.
[37] Ali U, Karim KJBA, Buang NA. A Review of the Properties and Applications of Poly (Methyl Methacrylate) (PMMA). Polymer Reviews. 2015;55(4):678-705.
[38] Zhao Y, Chun Wang C, Min Huang W, Purnawali H. Buckling of poly(methyl

methacrylate) in stimulus-responsive shape recovery. Appl Phys Lett. 2011;99(13):131911.
[39] Zhao Y, Huang WM, Wang CC. Thermo/chemo-responsive shape memory effect for micro/nano surface patterning atop polymers. Nanosci Nanotechnol Lett. 2012;4(9):862-78.
[40] Lu H, Huang WM, Wu XL, Ge YC, Zhang F, Zhao Y, et al. Heating/ethanol-response of poly methyl methacrylate (PMMA) with gradient pre-deformation and potential temperature sensor and anti-counterfeit applications. Smart Mater Struct. 2014;23(6):067002.
[41] Kim YY, Huang Q, Krishnaswamy S. Selective growth and ordering of self-assembly on metal/polymer thin-film heterostructures via photothermal modulation. Appl Phys Lett. 2010;96(12):123116.
[42] Fang TH, Chang WJ, Lin CM. Nanoindentation characterization of ZnO thin films. Mater Sci Eng, A. 2007;452-453:715-20.
[43] Fu YQ, Luo JK, Du XY, Flewitt AJ, Li Y, Markx GH, et al. Recent developments on ZnO films for acoustic wave based bio-sensing and microfluidic applications: a review. Sensors Actuators B: Chem. 2010;143(2):606-19.
[44] He XL, Li DJ, Zhou J, Wang WB, Xuan WP, Dong SR, et al. High sensitivity humidity sensors using flexible surface acoustic wave devices made on nanocrystalline ZnO/polyimide substrates. J Mater Chem C. 2013;1(39):6210-15.
[45] Chen J, Guo H, He X, Wang W, Xuan W, Jin H, et al. Development of flexible ZnO thin film surface acoustic wave strain sensors on ultrathin glass substrates. J Micromech Microeng. 2015;25(11):115005.
[46] Zhang DH, Yang TL, J.Ma, Wang QP, Gao RW, Ma HL. Preparation of transparent conducting ZnO:Al films on polymer substrates by r. f. magnetron sputtering. Appl Surf Sci. 2000;158:43-8.
[47] Lee JH. Effects of sputtering pressure and thickness on properties of ZnO:Al films deposited on polymer substrates. J Electroceram. 2008;23(2-4):512-18.
[48] Zhao Y, Huang WM, Fu YQ. Formation of micro/nano-scale wrinkling patterns atop shape memory polymers. JMiMi. 2011;21(6):067007.
[49] Huang WM, Yang B, Fu YQ. Polyurethane shape memory polymers. London: Taylor & Francis/CRC Press; 2012.
[50] Lee TRHaI. Wrinkle-Free Nanomechanical Film: Control and Prevention of Polymer Film Buckling. Nano Lett. 2007;7(2):372-9.
[51] Chung JY, Nolte AJ, Stafford CM. Surface wrinkling: a versatile platform for measuring thin-film properties. Adv Mater. 2011;23(3):349-68.
[52] Jia H, Wang S, Goudeau P, Li L, Xue X. Investigation of buckling transition from straight-sided to telephone-cord wrinkles in Al films. JMiMi. 2013;23(4):045014.
[53] Yu S, Zhang X, Xiao X, Zhou H, Chen M. Wrinkled stripes localized by cracks in metal films deposited on soft substrates. Soft matter. 2015;11(11):2203-12.
[54] Yu S, Sun Y, Ni Y, Zhang X, Zhou H. Controlled Formation of Surface Patterns

in Metal Films Deposited on Elasticity-Gradient PDMS Substrates. ACS applied materials & interfaces. 2016;8(8):5706-14.
[55] Yang S, Khare K, Lin P-C. Harnessing Surface Wrinkle Patterns in Soft Matter. Adv Funct Mater. 2010;20(16):2550-64.

Figures (Fig. 1-Fig. 12):

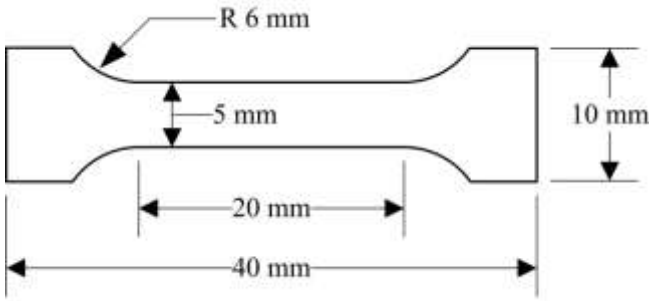

Fig. 1. Dimensions of sample of PMMA substrate.

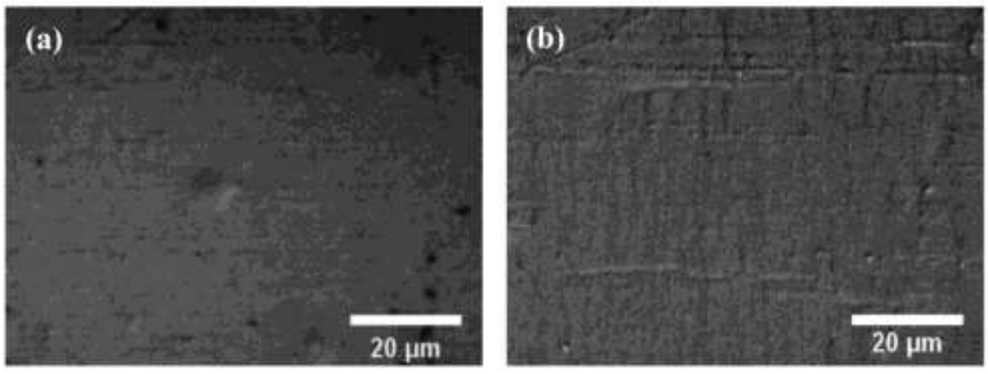

Fig. 2. Optical micrographs of sample 3 (a) before annealing; (b) after annealing.

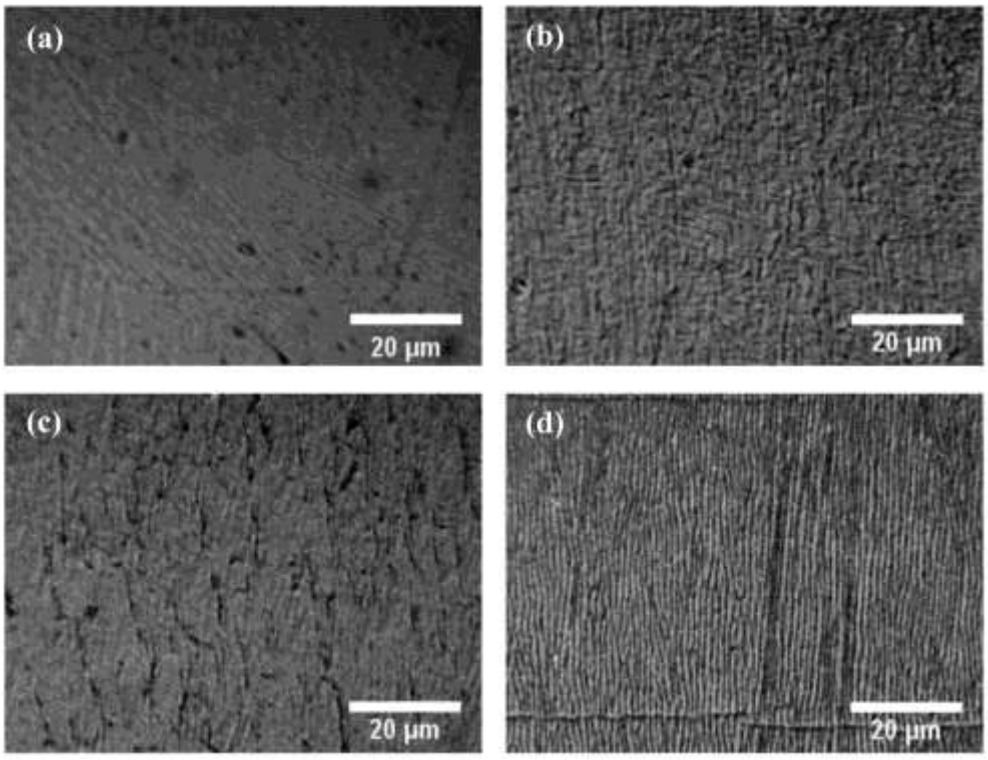

Fig. 3. Optical micrographs of (a) sample 4 before annealing; (b) sample 4 after annealing; (c) sample 5 after annealing; (d) sample 6 after annealing.

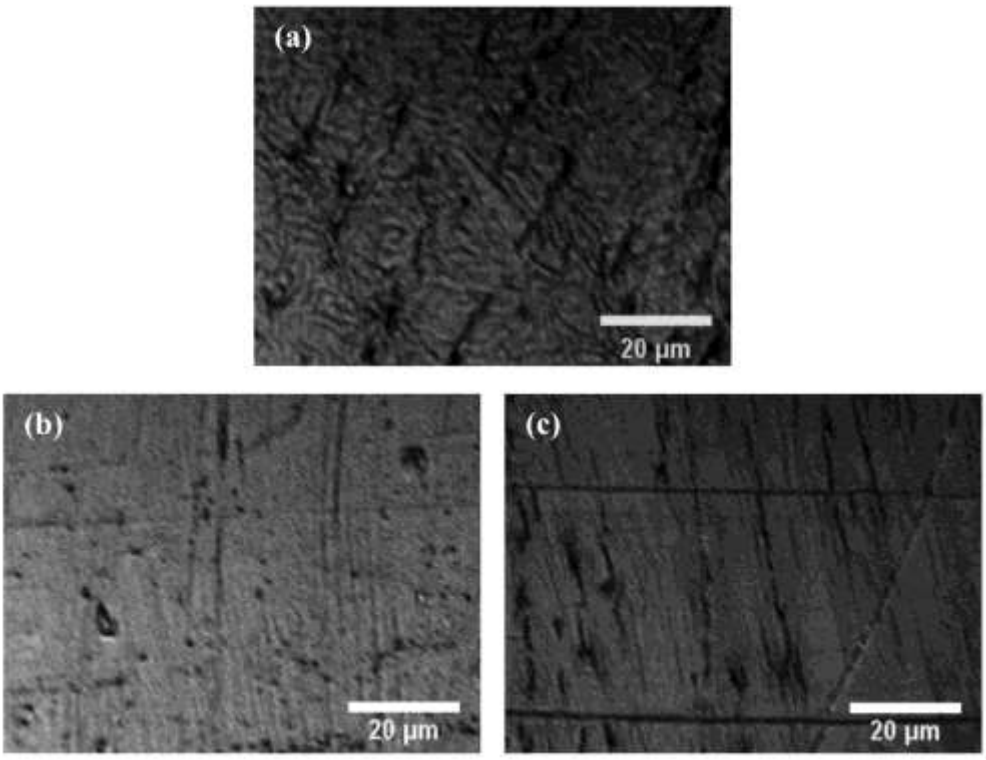

Fig. 4. Optical micrographs of (a) sample 7; (b) sample 8; (c) sample 9; after annealing.

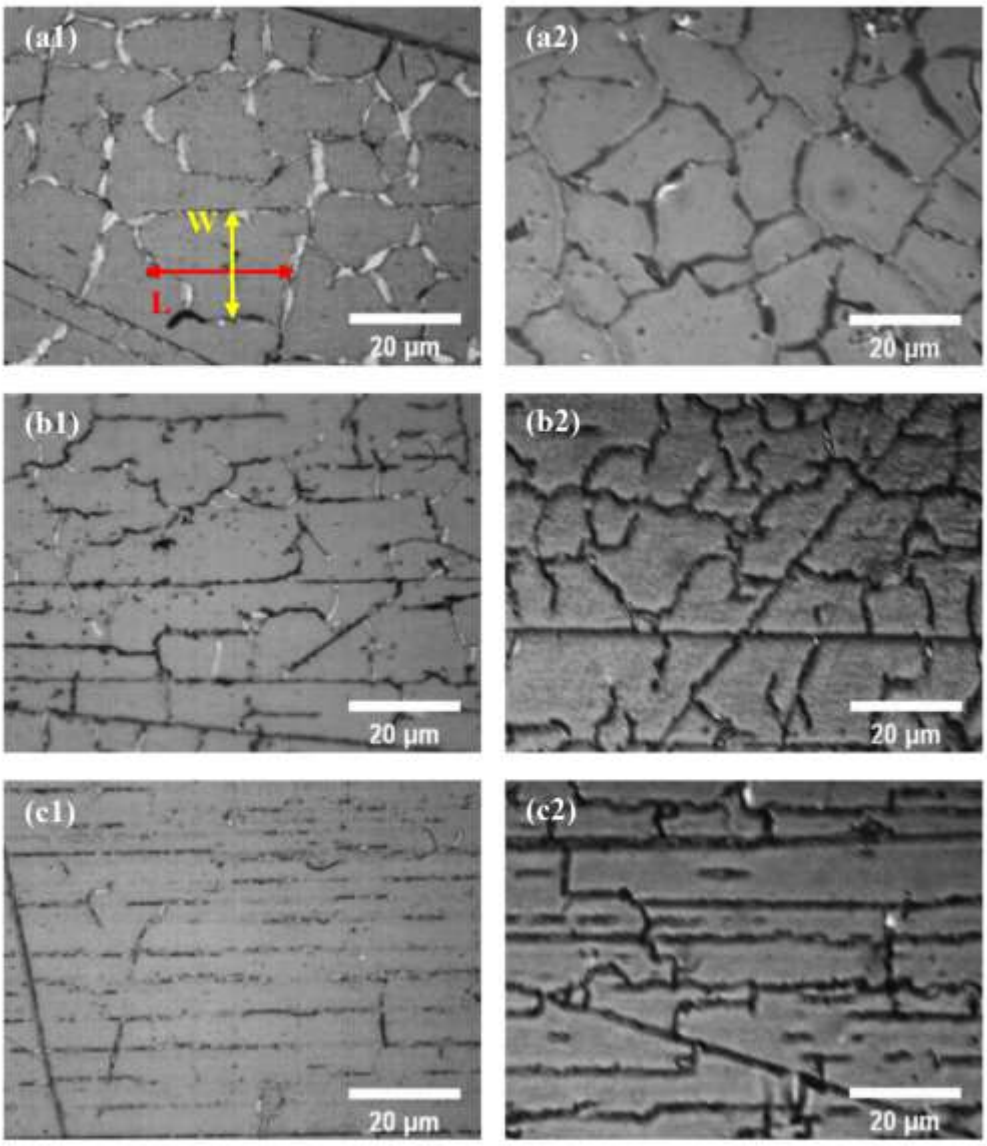

Fig. 5. Optical micrographs of (a) sample 10; (b) sample 11; (c) sample 12; (1) before annealing and (2) after annealing.

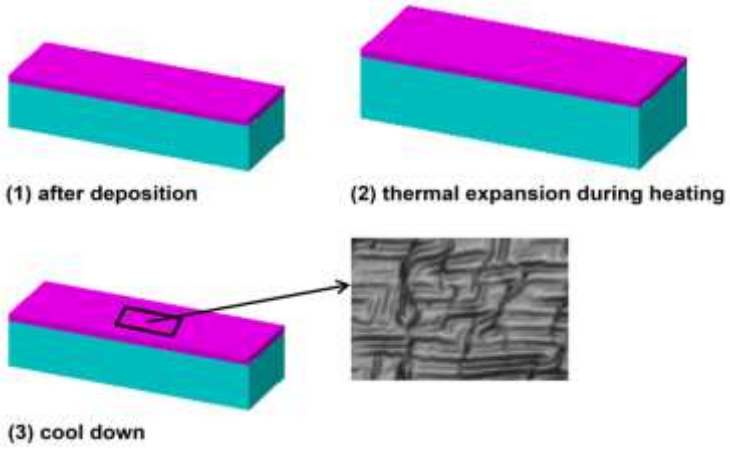

Fig. 6. Wrinkle generated on un-stretched samples by the thermal expansion mismatch.

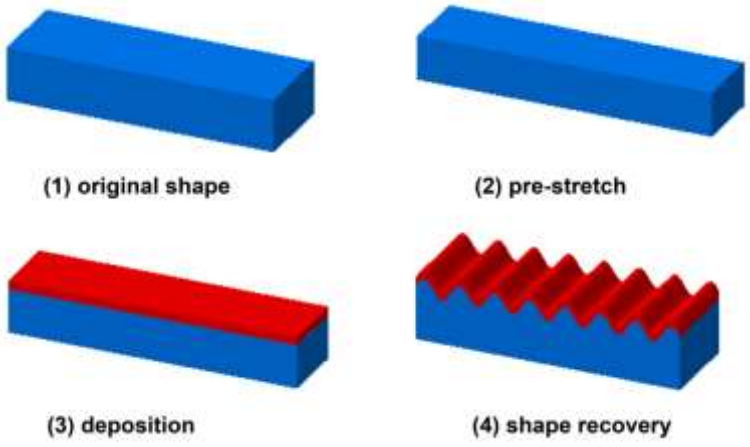

Fig. 7. Wrinkle formed in pre-stretched samples by the SME.

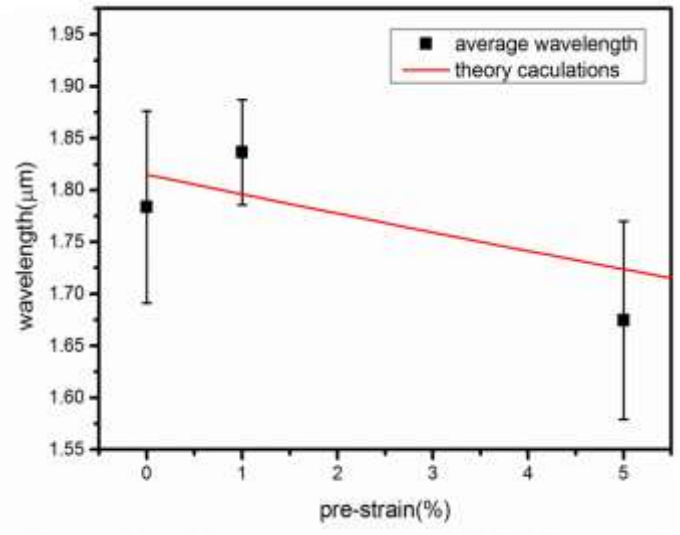

Fig. 8. The average wavelength versus the applied pre-strain.

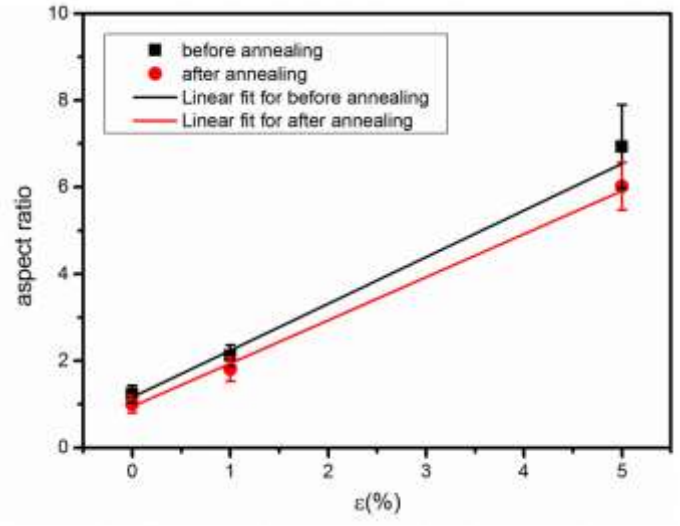

Fig. 9. The aspect ratio of closed domains in ZnO film occurred before and after annealing.

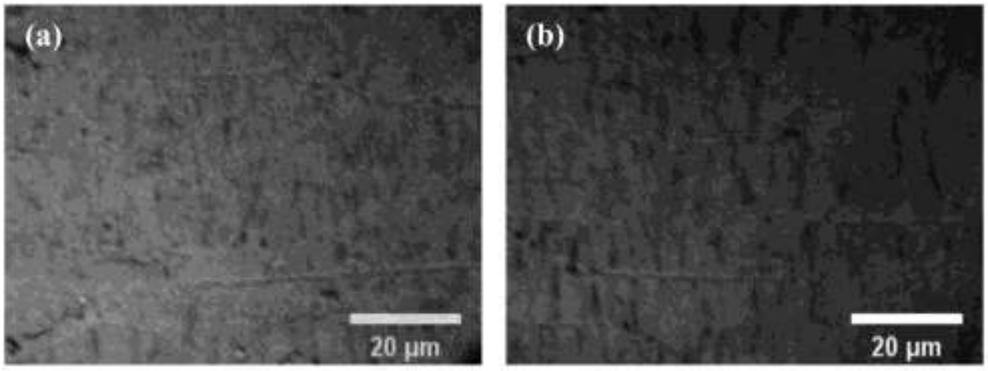

Fig. 10. Evolution of surface morphologies of sample 3 after soaking in ethanol for (a) 2 hours; (b) 36 hours.

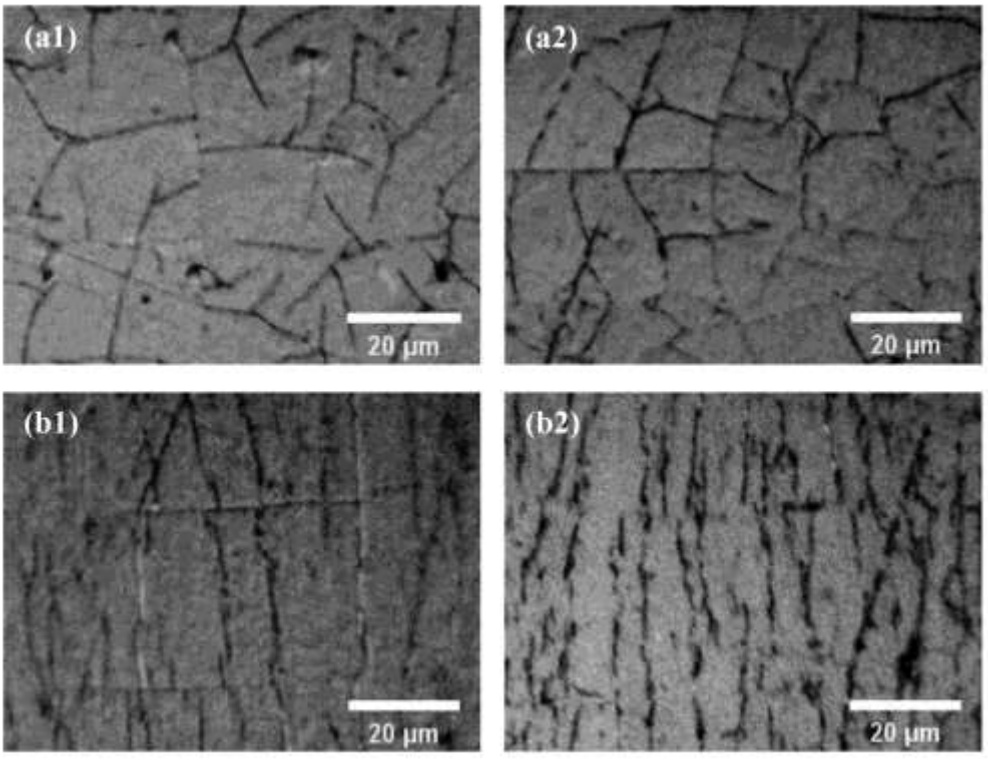

Fig. 11. Evolution of surface morphologies of (a) sample 4; (b) sample 6; after soaking in ethanol for (1) 2 hours; (2) 36 hours.

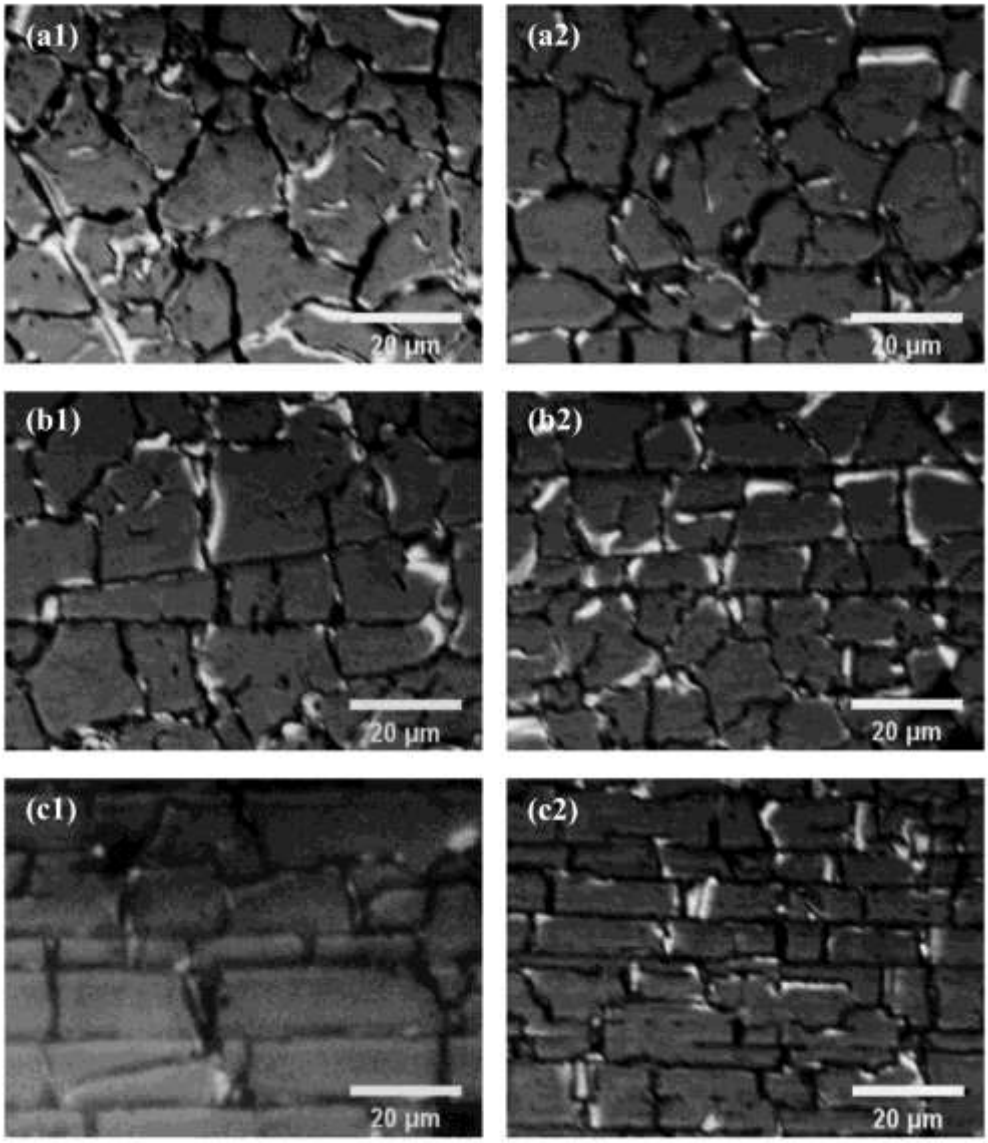

Fig. 12. Evolution of surface morphologies of (a) sample 10; (b) sample 11; (c) sample 12; after soaking in ethanol for (1) 2 hours; (2) 36 hours.

Table:

Table 1. Pre-strain and thickness of ZnO film of the samples.

Number	Thickness of ZnO film (nm)	Pre-strain (%)	Number	Thickness of ZnO film (nm)	Pre-strain (%)
sample 1	5	0	sample 7	30	0
sample 2	5	1	sample 8	30	1
sample 3	5	5	sample 9	30	5
sample 4	15	0	sample 10	45	0
sample 5	15	1	sample 11	45	1
sample 6	15	5	sample 12	45	5